Carbon 153 (2019) 189–195

Contents lists available at ScienceDirect

Carbon

journal homepage: www.elsevier.com/locate/carbon

# Reversibly compressible and freestanding monolithic carbon spherogels

Miralem Salihovic [a], Gregor A. Zickler [a], Gerhard Fritz-Popovski [b], Maike Ulbricht [c, d], Oskar Paris [b], Nicola Hüsing [a], Volker Presser [c, d], Michael S. Elsaesser [a, *]

[a] Chemistry and Physics of Materials, University of Salzburg, 5020 Salzburg, Austria
[b] Institute of Physics, Montanuniversitaet Leoben, 8700 Leoben, Austria
[c] INM – Leibniz Institute for New Materials, 66123 Saarbrücken, Germany
[d] Saarland University, 66123 Saarbrücken, Germany

ARTICLE INFO

*Article history:*
Received 9 April 2019
Received in revised form
17 June 2019
Accepted 26 June 2019
Available online 2 July 2019

*Keywords:*
Nanoporous carbon
Hollow sphere
Reversibly compressible materials
Sol-gel

ABSTRACT

We present a versatile strategy to tailor the nanostructure of monolithic carbon aerogels. By use of an aqueous colloidal solution of polystyrene in the sol-gel processing of resorcinol-formaldehyde gels, we can prepare, after supercritical drying and successive carbonization, freestanding monolithic carbon aerogels, solely composed of interconnected and uniformly sized hollow spheres, which we name carbon spherogels. Each sphere is enclosed by a microporous carbon wall whose thickness can be adjusted by the polystyrene concentration, which affects the pore texture as well as the mechanical properties of the aerogel monolith. In this study, we used monodisperse polystyrene spheres of approximately 250 nm diameter, which result in an inner diameter of the final hollow carbon spheres of approximately $200 \pm 5$ nm due to shrinkage during the carbonization process. The excellent homogeneity of the samples, as well as uniform sphere geometries, are confirmed by small- and angle X-ray scattering. The presence of macropores between the hollow spheres creates a monolithic network with the benefit of being reversibly compressible up to 10% linear strain without destruction. Electrochemical tests demonstrate the applicability of ground and $CO_2$ activated carbon spherogels as electrode materials.



## 1. Introduction

Tailored porous carbon materials, especially with controllable and uniform pore characteristics [1], are of high interest for energy storage [2,3], drug delivery [4], separation or gas adsorption applications [5]. In particular, a network build-up of hollow spheres with deliberately tailored sizes has several benefits due to the high surface-to-volume ratio, possibilities for encapsulation, and chemical stability [6]. Hollow carbon sphere powders have been prepared via polystyrene templating or by use of Stöber silica particles as scaffolds during hydrothermal processing of monosaccharides [7–10]. Polystyrene spheres as templates and resorcinol-formaldehyde were used to produce mesoporous carbon foams [11]. Close-packed polystyrene spheres can be infiltrated by a carbon source followed by carbonization, which results in periodic porous carbons [12–15]. In a pioneering work, the gelation of resorcinol-formaldehyde in ordered mesopores of silica was shown to result in structured carbon replicas of hexagonally ordered fiber bundles (CMK-3) [16]. In a soft-templating approach, dissolved polystyrene and mesophase pitch were processed via evaporation-induced phase separation to create meso/macroporous carbons [17]. Other routes for the synthesis of carbon materials composed of hollow spheres are based on a rapid ultrasonic treatment of a resorcinol-formaldehyde sol [18,19], a modified Stöber process [20], or chemical vapor deposition (CVD) on self-assembled polystyrene spheres [21]. By use of a CVD process involving ferrocene on silica, annealing and silica etching, hollow carbon sphere materials with uniform geometries (shell thickness of 30 nm) can be obtained [22]. The inner volume enclosed in the hollow carbon spheres may be beneficial for many applications; for example, it can be used as a sulfur reservoir for Li–S batteries or encapsulate nanosized catalysts [23]. The addition of nanometer-sized species into the interior of carbon spheres, however, remains challenging. For example, a vapor phase infusion method was successfully applied [24]. We have shown in a previous study that the introduction of hollow

* Corresponding author.
*E-mail address:* michael.elsaesser@sbg.ac.at (M.S. Elsaesser).

https://doi.org/10.1016/j.carbon.2019.06.086

spheres into a carbon aerogel network by polystyrene templating has also a considerable impact on the mechanical properties (maximum compressive strength) [25]. A comprehensive preparation overview to hollow-sphere structured materials can be found elsewhere [26]. Careful control of the sphere morphology, chemical composition, and pore size distribution is beneficial for energy applications by improved electrolyte filling, enhanced ion mobility, and limited volumetric changes during charge/discharge cycling. The sol-gel reaction of resorcinol-formaldehyde to organic porous solids [27] shows severe limitations in structuring the nanoscale morphology of the gels by use of various influencing sol-gel parameters [28].

In this study, the synthesis of micro/macroporous carbon hollow spheres from polystyrene templating is combined with the preparation of carbon monoliths by simple sol-gel processing of resorcinol and formaldehyde. Contrary to conventional hollow carbon sphere (HCS) materials in powder form described in the literature [6], we obtain freestanding monolithic samples composed of a network of uniformly sized hollow carbon spheres. It is expected that these networks exhibit a very homogeneous structure with macropores formed bet-ween microporous carbon shells. The presence of macropores will have an impact on the mechanical properties of these RF-based gels, thus resulting in carbon materials exhibiting a reversibly compressible nature. In our previous work, we have already shown that small amounts of individual hollow spheres can act as templates for resorcinol-formaldehyde based carbon aerogels affecting the reversibly compressible character [25]. Electrochemical characterization, by use of the approach of Ref. [32], is outlined in the Supporting Information. Now, by a careful variation of the polystyrene sphere concentration, we demonstrate the control of the shell thickness, hollow sphere size, and sphere cohesion. To the contrary of previous reports on templated, powdered carbon materials [7,11] we achieve reversibly compressible monolithic, low-density (0.06 g/cm$^3$) carbon materials with very high control and variability of the pore structure. As a direct consequence, our templating strategy expands the possibility to tune the carbon aerogel structure in a wide range by the formation of well-defined meso/macropores both in the core of the spheres and between spherical particles in addition to microporous carbon shells. We investigate structural and mechanical properties by use of scanning and transmission electron microscopy (SEM and TEM), small-angle X-ray scattering (SAXS), nitrogen gas sorption, and mechanical compression testing. To demonstrate the principle suitability of the material for energy storage applications, we performed electrochemical investigations (cyclic voltammetry and galvanostatic charge/discharge cycling) on activated, ground and binder-treated electrodes.

## 2. Experimental section

### 2.1. Materials and synthesis

Aqueous monodisperse polystyrene (PS) colloidal solutions with a concentration of 2.0 wt%, 4.0 wt% and 7.2 wt% (final samples labeled CA_2, CA_4, and CA_7.2) were used as templating agents. The PS spheres (Supporting *Information*: 250.8 nm, 0.015 PdI, Fig. S1 and SEM image in Fig. S2), were prepared by emulsion polymerization of styrene with potassium persulfate (KPS) as initiator and polyvinylpyrrolidone (PVP) as a stabilizing agent, as described previously [29]. The as-prepared reaction mixture contained 4 wt% PS, and the other two emulsions were prepared by dilution with deionized water (W) or evaporation, respectively. Additionally, a proof of concept sample was prepared by use of a commercial, 50 nm sized PS solution (ABCR, 1.5 wt%). 25 g of each PS solution was provided in a beaker followed by the addition of 1.25 g resorcinol (R; molar ratio R/W = 0.008) and 1.84 g formaldehyde solution (37 wt%, F (stabilized with methanol); molar ratio R/F = 0.5) as a sol. We used 25 g of distilled water for the CA reference sample without PS templating. The initial resorcinol substitution was catalyzed by sodium carbonate ($Na_2CO_3$; molar ratio R/C = 50) while for the condensation process we adjusted the pH value to 5.45 by dropwise addition of nitric acid ($HNO_3$). The gelation and aging to cylindrical RF/PS aquagel monoliths were performed by pouring the sol/PS solution into glass vessels, followed by storage of the gels for seven days at 80 °C. Afterwards, the RF/PS aquagels were immersed in an acetone bath (100 mL), repeated three times within three days, to allow a sufficient solvent exchange. These organogels were dried with supercritical $CO_2$ in an autoclave (Parr Instruments) with a volume of 300 mL at 12 MPa and 60 °C. Subsequently, the RF/PS specimen were carbonized in a tube furnace at 800 °C under argon gas. A further carbon spherogel sample series was synthesized for mechanical and electrochemical performance investigations by the use of a 1.5 wt%, 3.0 wt%, and 6.0 wt% PS solution (PS average sphere size: 273 nm; 0.030 PdI; labeled CA_1.5, CA_3, and CA_6) following the same protocol. Prior to electrochemical characterization, these carbon spherogels were physically activated by a constant flow of $CO_2$ in a tube furnace at 925 °C for 2 h.

### 2.2. Materials characterization

The morpholgy of the carbon spherogels was analyzed with a Zeiss Ultra Plus field emission scanning electron microscope (SEM) using an in-lens secondary electron detector. The acceleration voltage was adjusted between 2 kV and 5 kV. Transmission electron microscope (TEM) images were recorded with a JEOL JEM F200 TEM, which is equipped with a cold field emission source, using a TVIPS F216 2k by 2k CMOS camera. An accelerating voltage of 200 kV was used. Thermogravimetric analysis (TGA) was carried out with a NETZSCH STA 449 F3 Jupiter device from 20 °C to 1000 °C with a heating rate of 10 °C min$^{-1}$ using an argon or synthetic air atmosphere.

Nitrogen adsorption isotherms were obtained with a Quantachrome iQ sorption apparatus at −196 °C. Degassing of the samples was conducted at 300 °C for 12 h. By use of quenched solid density functional theory (QSDFT) the specific surface areas (SSA) and pore size distributions (PSD) were calculated. Dynamic light scattering (DLS) and zeta potential measurements were performed with a Malvern Zetasizer instrument. A light-backscattering angle of 173° was adjusted to record the data. Each measurement contains 30 separate DLS measurements with 3 sub-runs each of 10 s duration.

Small angle X-ray scattering (SAXS) was done on a NANO-STAR laboratory instrument (Bruker AXS), equipped with an IμS microsource (Incoatec) using Cu-Kα radiation and 300 μm SCATEX pinholes (Incoatec). The scattering patterns were measured using a VÅNTEC-2000 detector (Bruker AXS) at sample-detector distances of 1052 mm and 675 mm in order to cover a wide angular range. Distances were calibrated by a silver-behenate standard [30]. 4 to 17 points of each specimen were sampled to check for inhomogeneities of the structural parameters across the samples. Transmission of the samples was determined for each measurement point, and a background scattering pattern detected without the samples was subtracted after correction for transmission effects. One dimensional scattering I(q) curves were computed from the two-dimensional scattering patterns, where $I$ is the measured intensity, and $q = 4\pi/\lambda \cdot \sin(\theta/2)$ is the length of the scattering vector, which depends on the scattering angle $\theta$, and the wavelength $\lambda$ of the X-rays. The one-dimensional (1D) scattering curves measured at the two detector positions were merged. The SAXS

data were modeled theoretically by using a core-shell model [31]. This model was modified to include micropores in the walls of the hollow spheres by assuming spherical micropores with a Gaussian diameter distribution (see section "SAXS Model" in Supporting *Information*).

The mechanical properties of the samples were investigated by compression tests on a uniaxial universal testing machine (Zwick/Roell Z-250) equipped with a 1 kN load cell. Each test cycle consisted of 5 times repeated compression up to 10% strain at a rate of 5 mm $min^{-1}$. The compressive Young's modulus was determined according to our previous study [25].

## 3. Results and discussion

Our study comprises the build-up of monolithic carbon aerogels composed only out of hollow spheres as a result of resorcinol-formaldehyde gelation around PS templates, which we call spherogels. We varied the concentration of aqueous colloidal polystyrene solutions (2.0 wt%, 4.0 wt%, and 7.2 wt%) as templating agents and labeled these sphero-gels as CA_2, CA_4, and CA_7.2 as well as a (pristine) reference sample without PS templating (by use of an equal volume of distilled water). Thereby, we were able to modify the network build-up of monolithic carbon aerogels after carbonization of the supercritically dried resorcinol-formaldehyde/polystyrene material (Fig. 1).

Apparently, the negatively charged outer surface of the PS spheres (as confirmed by the negative Zeta potential of −18.5 mV, Supporting *Information*, Fig. S1B) is a preferred location for the resorcinol-formaldehyde substitution reaction, thus resulting in perfectly RF enclosed polystyrene spheres after gelation (Fig. 2). Carbonization results in a slight linear shrinkage of the monoliths of 20%, resulting in a bulk density of 0.06 g $cm^{-3}$ for all samples. Similar to our previous investigation about reversibly compressible carbon aerogels [25], we also use a low resorcinol-to-water molar ratio of 0.008. As seen in Fig. 3, the morphology of the final carbon materials is shown via scanning (SEM) and transmission (TEM) electron microscopy. Careful adjustment of the selected polystyrene concentrations in combination with a fixed resorcinol-formaldehyde molar ratio yields a gel microstructure composed solely out of spheres. As shown by the SEM images as seen in Fig. 3A–C, the carbon shell of each sphere is partially fused with the shell of neighboring spheres at a low initial polystyrene concentration. In the case of higher polystyrene concentrations, the spheres appear more isolated, sharing only a small overlap. The corresponding TEM micrographs (Fig. 3D–F) reveal the ability of our approach to create monolithic carbon spherogels with homogeneously sized hollow spheres and adjustable wall thicknesses by use of varying polystyrene concentrations. A low polystyrene concentration (2 wt%) yields spheres with 94 ± 2 nm wall thickness, and higher polystyrene concentrations result in lower wall thicknesses of 45 ± 1 nm or 18 ± 2 nm for 4 wt% and 7.2 wt%, respectively. The diameter of the hollow core remains constant with approximately 200 nm, with variations of less than 3% for all concentrations (Table 1).

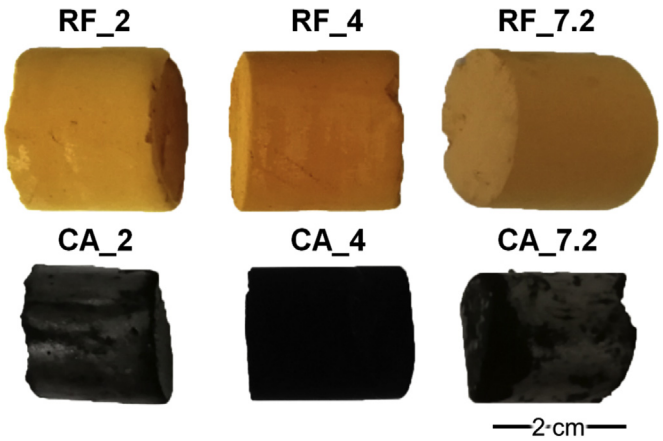


**Fig. 1.** Photograph of monolithic, cylindrical RF/PS spherogels (upper row) and corresponding carbon samples (lower row) with varied PS concentrations in the starting solution (2 wt%, 4 wt%, and 7.2 wt%). (A colour version of this figure can be viewed online.)

The concurrently occurring decomposition of polystyrene and carbonization of resorcinol-formaldehyde not only allows for the formation of hollow carbon spheres but also yields intact monolithic structures composed of interconnected hollow particles (Supporting Information, Figs. S2–S4). To confirm the homogeneity of the diameters of the spheres for macroscopic sample quantities, we performed small-angle X-ray scattering (SAXS) measurements. The scattering curves of all core-shell samples show pronounced oscillations (Fig. 4). The positions of the minima are directly related to the shell thickness t, while the number of observable minima is mainly determined by smearing of higher orders due to polydispersity. The oscillations are completely absent in the non-templated reference sample. Fitting a model to the experimental SAXS curves measured at different positions within the monoliths resulted in essentially the same mean thickness (Table 1). The width of the size distribution is estimated to be $\Delta t/t \approx 5\%$ from the number of visible minima. The curves show also a weak shoulder at $q \approx 2.5\ nm^{-1}$, which is attributed to the presence of micropores; the fit gives a mean radius of 0.4 nm (Table 1). This suggests a very high degree of homogeneity of the shell thicknesses within each monolith and the presence of ultramicropores in the pore walls. While shell thickness obtained from TEM and SAXS agree very well for the samples Ca_4 and CA_7.2, there is a significant difference of the shell thicknesses obtained for CA_2 (Table 1). This is somehow surprising, as both methods are very sensitive to the shell thickness. Tentatively, we attribute this to a gradient in the density (and thus the scattering contrast) within the shell for this sample. Indeed, a decreasing density (due to, e.g., an increasing micropore amount) from the inner to the outer side of the shell would be consistent with the experimental findings and will be subject to further investigations.

Nitrogen adsorption isotherms at −196 °C (Fig. 5A) of the carbon samples were recorded to investigate the pore size distribution (Fig. 5B), as well as the specific surface areas and the micropore volume (Table 1). The type IV isotherms for the spherogels CA_2, CA_4, and CA_7.2 with a hysteresis loop H4 correspond well to the microstructure of the sample with macropores enclosed by a microporous particle network. The isotherms also show the tensile strength effect (TSE) [33–35], that is, the sudden evaporation of nitrogen from the sphere interior is clearly indicated by the sharp drop in the desorption isotherm at $p/p_0$ of 0.5. The shape of the isotherms of CA_2 and CA_4, indicates the presence of micro- and macropores only, while CA_7.2 and the carbon aerogel reference sample without polystyrene templating seem to contain also some intermediate mesopores. While micropores are located in the carbon shells, the macropores originate from the hollow core, and the mesopores are probably connected to the pores between the hollow spheres. The filling of the uniform 200 nm inner volume of the spheres is clearly seen in the isotherms by the sharp adsorbed volume increase at relative pressures close to one. The micropore generation occurs during carbonization (evaporation of H- and O-compounds) with a micropore volume in the range of 0.2 $cm^3\ g^{-1}$. Applying the quenched solid density functional theory (QSDFT) and assuming slit-shaped pores, we obtain a specific surface area of

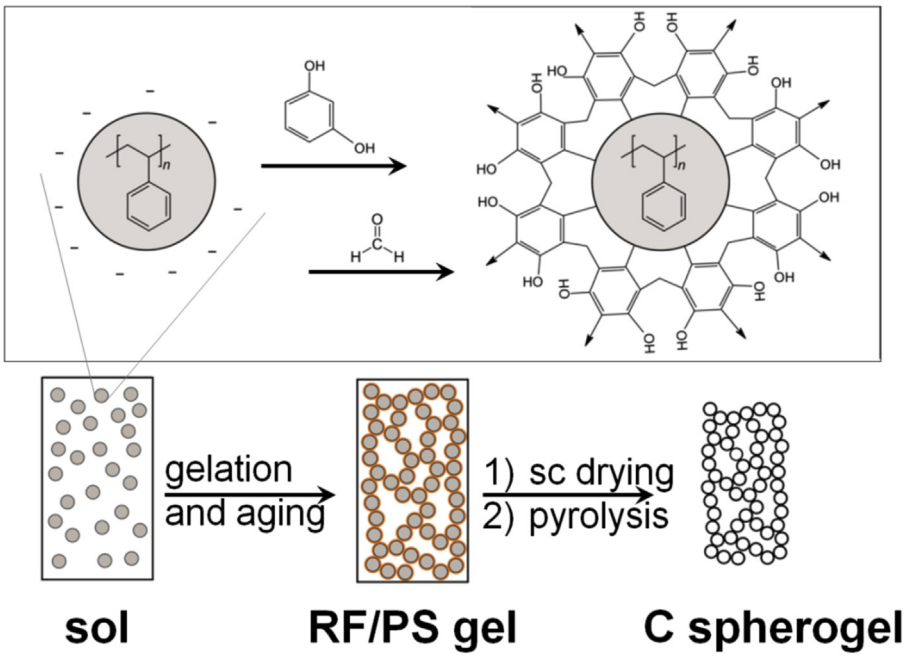


**Fig. 2.** Schematic representation of the synthesis of carbon spherogels that are composed solely of hollow spheres starting from polystyrene colloids and resorcinol and formaldehyde as carbon sources (sc = supercritical drying). (A colour version of this figure can be viewed online.)

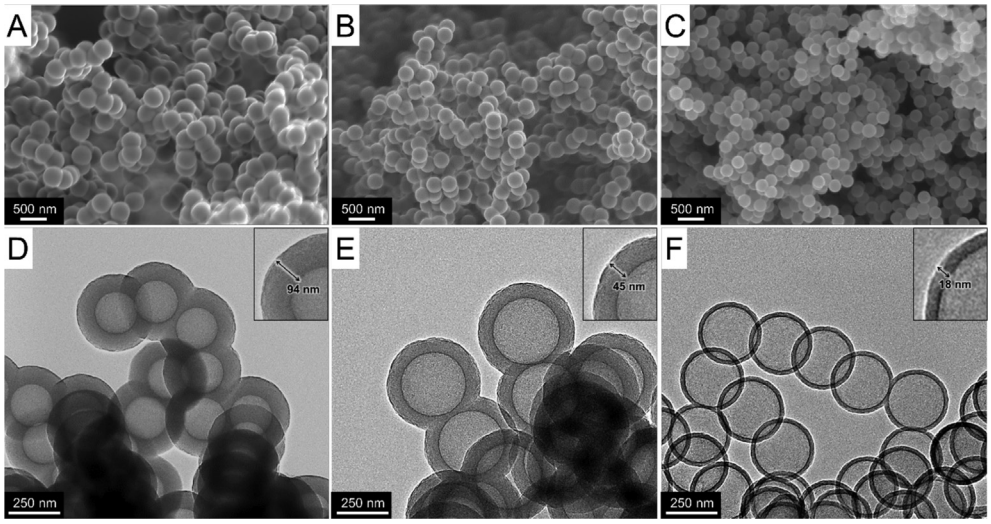


**Fig. 3.** Scanning electron micrographs (A–C) and corresponding transmission electron micrographs (D–F) of polystyrene-templated carbon spherogels with 2 wt% (CA_2), 4 wt% (CA_4), and 7.2 wt% polystyrene (CA_7.2) as the templating agent.

**Table 1**
Physical and geometric properties of carbon spherogels templated with different polystyrene concentrations, including the reference sample (without polystyrene addition) obtained from $N_2$ sorption, TEM micrographs, and data calculated from SAXS measurements.

| Sample | SSA(QSDFT) | Inner diameter[a](TEM) | Wall thickness[a](TEM) | Wall thickness(SAXS) | Micropore diameter (SAXS) | Specific pore volume[b](QSDFT) | Micropore volume[c](QSDFT) | $\varrho_{bulk}$ |
|---|---|---|---|---|---|---|---|---|
| | ($m^2$/g) | (nm) | (nm) | (nm) | (nm) | ($cm^3$/g) | ($cm^3$/g) | (g/$cm^3$) |
| Reference | 584 | – | – | – | – | 0.44 | 0.17 | 0.06 ± 0.01 |
| CA_2 | 612 | 196 ± 3 | 94 ± 2 | 78 ± 0.3 | 0.76 ± 0.02 | 0.21 | 0.18 | 0.06 ± 0.01 |
| CA_4 | 667 | 200 ± 5 | 45 ± 1 | 48 ± 0.9 | 0.78 ± 0.04 | 0.26 | 0.19 | 0.06 ± 0.01 |
| CA_7.2 | 680 | 202 ± 3 | 18 ± 1 | 18 ± 0.6 | 0.72 ± 0.06 | 0.43 | 0.20 | 0.06 ± 0.01 |

[a] Determination of the inner diameter and wall thickness by evaluation of transmission electron micrographs of 15 spheres.
[b] <30 nm.
[c] <2 nm.

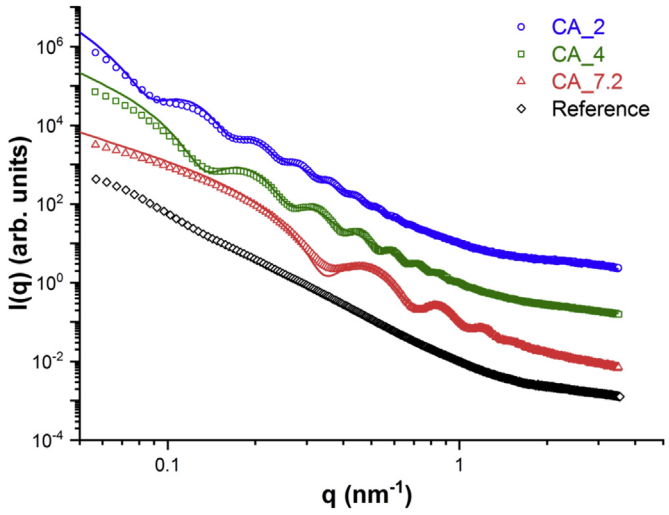


**Fig. 4.** SAXS curves of CA_2, CA_4, CA_7.2, and reference (no templating). The curves are vertically shifted for better visibility. (A colour version of this figure can be viewed online.)

580–680 $m^2g^{-1}$ for our samples with an increase of the total pore volume from 0.21 $cm^3\,g^{-1}$ (CA_2) to 0.43 $cm^3\,g^{-1}$ (CA_7.2), which we consider as a result of a clearly higher overall interior volume as well as an increased number of pores between spheres for CA_7.2.

Our synthesis strategy further allows generating spherogels with hollow sphere dimensions in the mesopore range. By use of polystyrene spheres with 50 nm and a concentration of 1.5 wt%, we prepared a hierarchically structured carbon aerogel composed of hollow spheres with an inner diameter of roughly 40 nm and a shell thickness of 13 nm (TEM image in Supporting *Information*, Fig. S5). In this case a commercial PS dispersion was used, apparently exhibiting a broader size distribution, which is reflected in a carbon spherogel consisting out of hollow spheres with an inner diameter in the range of 35–45 nm. A corresponding nitrogen adsorption analysis shows the pronounced hysteresis loop type H4 with a sharp drop at $p/p_0$ at 0.5, indicating the TSE and the flexible adaptability of our route to different PS systems. Calculation of the SSA and pore volume resulted in 620 $m^2\,g^{-1}$ and 0.6 $cm^3\,g^{-1}$, respectively.

We investigated the structure of the carbon spherogels by Raman spectroscopy. The Raman spectra feature for all samples the presence of a D-mode at ~1345 $cm^{-1}$ and a G-mode at ~1584 $cm^{-1}$ with a full-width half maximum of 11 $cm^{-1}$ and ~60 $cm^{-1}$, respectively, and thus verifies the incomplete crystalline character. This is supported by an $I_D/I_G$ of about 0.86 for all samples including the non-templated (pristine) carbon aerogel (Supporting *Information*, Fig. S6, and Table S1) and has been reported similarly on resol-based carbon aerogels [36,37].

To explore the mechanical properties of the spherogels, we prepared an additional series of polystyrene-templated CAs by use of 1.5 wt%, 3 wt%, and 6 wt% PS with a comparable sphere diameter of 273 ± 8 nm (SEM micrograph analysis). The impact of PS concentration, accompanied by the number of hollow spheres in the CA and the content of macropores, on the mechanical properties of the CAs was investigated by a five-times repeated compression test up to 10% strain for each sample (Supporting *Information*, Fig. S7). As depicted in Fig. 6, after increasing the PS concentration from 1.5% to 6%, we observe a stiffening of the samples, indicated by an increase in the compressive modulus of the samples from 0.086 MPa to 0.149 MPa. Thus, the CA_6 sample with lower macropore content shows a nearly three times stiffer behavior than the pristine reference.

We further explored the suitability of carbon spherogels for

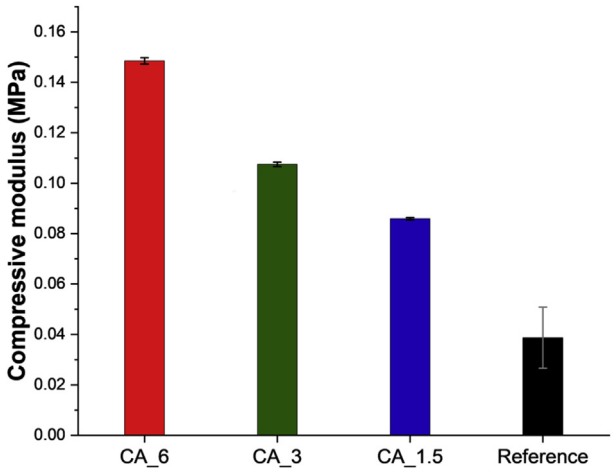


**Fig. 6.** Bar chart illustrating the compressive moduli of spherogel monoliths with decreasing sol PS concentrations (CA_6: 6 wt% PS; CA_3: 3 wt% PS; CA_1.5: 1.5 wt% PS) and pristine reference sample (black). The average of 5 compression cycles up to 10% strain, and the standard deviation error bar are shown. (A colour version of this figure can be viewed online.)

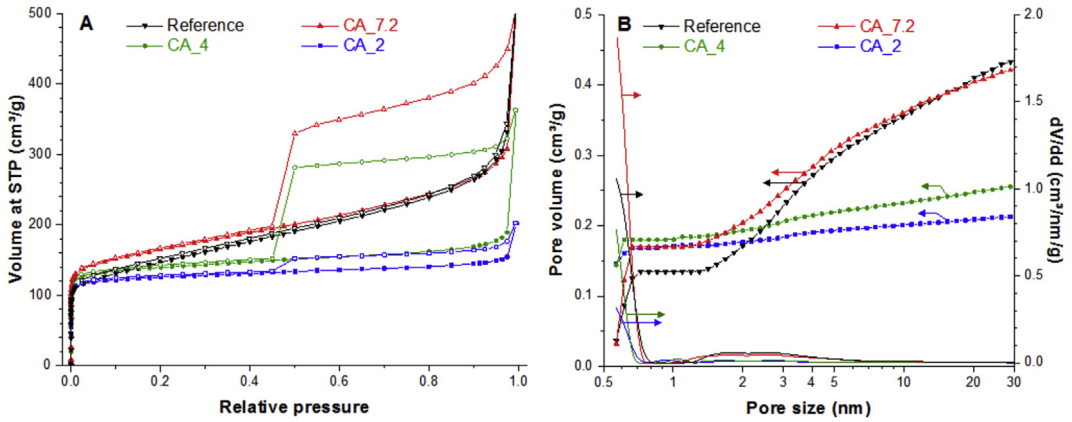


**Fig. 5.** (A) Nitrogen sorption isotherms measured at −196 °C and (B) cumulative pore size distributions (symbols, left axis) and differential pore size distribution (lines, right axis) for carbon spherogels with different polystyrene concentrations and the pristine reference sample. Pore size distributions were determine using QSDFT assuming slit pore geometry. (A colour version of this figure can be viewed online.)

electrochemical applications, in particular, for potential use as electrodes in supercapacitors. We performed first electrochemical investigations by the use of activated and ground monoliths, as well as polymer-treated electrodes. Carbon spherogel samples CA_1.5, CA_3, and CA_6 (and pristine sample) were physically activated [38] with $CO_2$ at 925 °C with the result of an increase of the SSA to the range of 1681–1861 $m^2 g^{-1}$. Concomitant, the total pore volume was extended up to 1.1 $cm^3 g^{-1}$, and the micropore volume increased to 0.74 $cm^3 g^{-1}$ (Supporting *Information*, Fig. S8, and Table S1). SEM images of the activated samples (Fig. S9) reveal that $CO_2$ treatment does not cause the collapse or other structural deterioration of the hollow spheres.

The general electrochemical performance of the crushed monolithic carbon electrodes (Supporting *Information*, Fig. S10) shows the ability of the material to be used as electrodes for electrical double-layer capacitors. For a common organic electrolyte, we have quantified the specific capacitance to be around 100 F $g^{-1}$, which is a value comparable to other activated carbon materials. Crushing the initially monolithic material was necessary to ensure a homogenous electrode thickness and optimized contact with the current collector; future work will explore the monolithic material as free-standing electrodes.

## 4. Conclusions

In the present work, we have demonstrated a facile route to monolithic carbon spherogels via polystyrene templating during resorcinol-formaldehyde sol-gel processing. The gels are solely composed of uniformly sized hollow carbon spheres, and the process shows great potential to control the pore diameters and wall thicknesses. We confirmed the excellent homogeneous of the monoliths as well as sphere size uniformity by SAXS and TEM measurements. The major advantages of this strategy towards these spherogels are 1) the advantages of mild reaction conditions during sol-gel processing, 2) the ease of modification of the synthesis protocol (e.g., a variation of the polystyrene concentration or resorcinol-formaldehyde amount), and 3) low cost and no equipment barriers.

By use of polystyrene spheres with varying sizes and concentrations, the wall thickness of the spheres as well as the inner volume is adjustable with a high level of control. Additionally, reversible compressibility up to 10% without destruction is shown, which can be related to the macropores enclosed between the hollow carbon spheres. Furthermore, we demonstrate for crushed carbon spherogels the principal suitability for electrochemical applications.

Our strategy can be extended to various functional carbon materials by the use of hybrid polystyrene capsules [39] with the aim to functionalize the inner volume with inorganic or metal nanoparticles. This would allow, for example, the use of nanosized inorganic species as intercalation components in combination with electrically conductive carbon for electrochemical applications.

## Acknowledgments

For financial support of this study, the Interreg V Programm-AB97 TFP-HyMat is kindly acknowledged. VP kindly thanks Eduard Arzt (INM) for his continuing support. Maurizio Musso and Andreas Reyer (University of Salzburg) are kindly acknowledged for Raman measurements. We thank Thomas Wimmer (FH Salzburg) for recording the compression test data. TEM measurements were carried out on a JEOL JEM F200 TEM which was funded by Interreg Österreich - Bayern 2014 - 2020 Programm-AB29 - "Synthese, Charakterisierung und technologische Fertigungsansätze für den Leichtbau "n2m" (nano-to-macro)".

## Appendix A. Supplementary data

Supplementary data to this article can be found online at https://doi.org/10.1016/j.carbon.2019.06.086.

## References

[1] M. Antonietti, N. Fechler, T.-P. Fellinger, Carbon aerogels and monoliths: control of porosity and nanoarchitecture via sol–gel routes, Chem. Mater. 26 (1) (2013) 196–210.
[2] V.G. Pol, M.M. Thackeray, Spherical carbon particles and carbon nanotubes prepared by autogenic reactions: evaluation as anodes in lithium electrochemical cells, Energy Environ. Sci. 4 (5) (2011) 1904–1912.
[3] J. Biener, M. Stadermann, M. Suss, M.A. Worsley, M.M. Biener, K.A. Rose, T.F. Baumann, Advanced carbon aerogels for energy applications, Energy Environ. Sci. 4 (3) (2011) 656–667.
[4] L. Zhang, M. Yao, W. Yan, X. Liu, B. Jiang, Z. Qian, Y. Gao, X.-j. Lu, X. Chen, Q.-l. Wang, Delivery of a chemotherapeutic drug using novel hollow carbon spheres for esophageal cancer treatment, Int. J. Nanomed. 12 (2017) 6759.
[5] C. Liang, Z. Li, S. Dai, Mesoporous carbon materials: synthesis and modification, Angew. Chem. Int. Ed. 47 (20) (2008) 3696–3717.
[6] T. Liu, L. Zhang, B. Cheng, J. Yu, Hollow carbon spheres and their hybrid nanomaterials in electrochemical energy storage, Adv. Energy Mater. 9 (17) (2019) 1803900.
[7] R.J. White, K. Tauer, M. Antonietti, M.-M. Titirici, Functional hollow carbon nanospheres by latex templating, J. Am. Chem. Soc. 132 (49) (2010) 17360–17363.
[8] N. Brun, K. Sakaushi, L. Yu, L. Giebeler, J. Eckert, M.M. Titirici, Hydrothermal carbon-based nanostructured hollow spheres as electrode materials for high-power lithium–sulfur batteries, Phys. Chem. Chem. Phys. 15 (16) (2013) 6080–6087.
[9] A.B. Fuertes, P. Valle-Vigon, M. Sevilla, One-step synthesis of silica@resorcinol-formaldehyde spheres and their application for the fabrication of polymer and carbon capsules, Chem. Commun. 48 (49) (2012) 6124–6126.
[10] S.B. Yoon, K. Sohn, J.Y. Kim, C.H. Shin, J.S. Yu, T. Hyeon, Fabrication of carbon capsules with hollow macroporous core/mesoporous shell structures, Adv. Mater. 14 (1) (2002) 19–21.
[11] W.W. Lukens, G.D. Stucky, Synthesis of mesoporous carbon foams templated by organic colloids, Chem. Mater. 14 (4) (2002) 1665–1670.
[12] A. Stein, Sphere templating methods for periodic porous solids, Microporous Mesoporous Mater. 44 (2001) 227–239.
[13] Y. Liu, J. Goebl, Y. Yin, Templated synthesis of nanostructured materials, Chem. Soc. Rev. 42 (7) (2013) 2610–2653.
[14] T.F. Baumann, J.H. Satcher Jr., Homogeneous incorporation of metal nanoparticles into ordered macroporous carbons, Chem. Mater. 15 (20) (2003) 3745–3747.
[15] T.F. Baumann, J.H. Satcher, Template-directed synthesis of periodic macroporous organic and carbon aerogels, J. Non-Cryst. Solids 350 (2004) 120–125.
[16] S. Jun, S.H. Joo, R. Ryoo, M. Kruk, M. Jaroniec, Z. Liu, T. Ohsuna, O. Terasaki, Synthesis of new, nanoporous carbon with hexagonally ordered mesostructure, J. Am. Chem. Soc. 122 (43) (2000) 10712–10713.
[17] P. Adelhelm, Y.S. Hu, L. Chuenchom, M. Antonietti, B.M. Smarsly, J. Maier, Generation of hierarchical meso-and macroporous carbon from mesophase pitch by spinodal decomposition using polymer templates, Adv. Mater. 19 (22) (2007) 4012–4017.
[18] V.G. Pol, L.K. Shrestha, K. Ariga, Tunable, functional carbon spheres derived from rapid synthesis of resorcinol-formaldehyde resins, ACS Appl. Mater. Interfaces 6 (13) (2014) 10649–10655.
[19] A.D. Dysart, X.L. Phuah, L.K. Shrestha, K. Ariga, V.G. Pol, Room and elevated temperature lithium-ion storage in structurally Tailored submicron carbon spheres with mechanistic Elucidation, Carbon 134 (2018) 334–344.
[20] J. Liu, S.Z. Qiao, H. Liu, J. Chen, A. Orpe, D. Zhao, G.Q. Lu, Extension of the Stöber method to the preparation of monodisperse resorcinol–formaldehyde resin polymer and carbon spheres, Angew. Chem. 123 (26) (2011) 6069–6073.
[21] G. Zheng, S.W. Lee, Z. Liang, H.-W. Lee, K. Yan, H. Yao, H. Wang, W. Li, S. Chu, Y. Cui, Interconnected hollow carbon nanospheres for stable lithium metal anodes, Nat. Nanotechnol. 9 (8) (2014) 618.
[22] Z. Lei, Z. Chen, X. Zhao, Growth of polyaniline on hollow carbon spheres for enhancing electrocapacitance, J. Phys. Chem. C 114 (46) (2010) 19867–19874.
[23] R.A. Ramli, Hollow polymer particles: a review, RSC Adv. 7 (83) (2017) 52632–52650.
[24] N. Jayaprakash, J. Shen, S.S. Moganty, A. Corona, L.A. Archer, Porous hollow carbon@sulfur composites for high-power lithium-sulfur batteries, Angew. Chem. Int. Ed. 50 (26) (2011) 5904–5908.
[25] M. Salihovic, N. Hüsing, J. Bernardi, V. Presser, M.S. Elsaesser, Carbon aerogels with improved flexibility by sphere templating, RSC Adv. 8 (48) (2018) 27326–27331.
[26] X. Lai, J.E. Halpert, D. Wang, Recent advances in micro-/nano-structured hollow spheres for energy applications: from simple to complex systems, Energy Environ. Sci. 5 (2) (2012) 5604–5618.
[27] R.W. Pekala, Organic aerogels from the polycondensation of resorcinol with formaldehyde, J. Mater. Sci. 24 (9) (1989) 3221–3227.
[28] A.M. Elkhatat, S.A. Al-Muhtaseb, Advances in tailoring resorcinol-

formaldehyde organic and carbon gels, Adv. Mater. 23 (26) (2011) 2887–2903.
[29] X. Du, J. He, Facile size-controllable syntheses of highly monodisperse polystyrene nano-and microspheres by polyvinylpyrrolidone-mediated emulsifier-free emulsion polymerization, J. Appl. Polym. Sci. 108 (3) (2008) 1755–1760.
[30] T. Huang, H. Toraya, T. Blanton, Y. Wu, X-ray powder diffraction analysis of silver behenate, a possible low-angle diffraction standard, J. Appl. Crystallogr. 26 (2) (1993) 180–184.
[31] J.S. Pedersen, Analysis of small-angle scattering data from colloids and polymer solutions: modeling and least-squares fitting, Adv. Colloid Interface Sci. 70 (1997) 171–210.
[32] D. Weingarth, M. Zeiger, N. Jäckel, M. Aslan, G. Feng, V. Presser, Graphitization as a universal tool to tailor the potential-dependent capacitance of carbon supercapacitors, Adv. Energy Mater. 4 (13) (2014) 1400316.
[33] S. Ikeda, K. Tachi, Y.H. Ng, Y. Ikoma, T. Sakata, H. Mori, T. Harada, M. Matsumura, Selective adsorption of glucose-derived carbon precursor on amino-functionalized porous silica for fabrication of hollow carbon spheres with porous walls, Chem. Mater. 19 (17) (2007) 4335–4340.
[34] J.C. Groen, L.A. Peffer, J. Pérez-Ramírez, Pore size determination in modified micro-and mesoporous materials. Pitfalls and limitations in gas adsorption data analysis, Microporous Mesoporous Mater. 60 (1–3) (2003) 1–17.
[35] M. Kruk, M. Jaroniec, Gas adsorption characterization of ordered organic–inorganic nanocomposite materials, Chem. Mater. 13 (10) (2001) 3169–3183.
[36] Z. Zhai, S. Wang, Y. Xu, L. Zhang, M. Yan, Z. Liu, Carbon aerogels with modified pore structures as electrode materials for supercapacitors, J. Solid State Electrochem. 21 (12) (2017) 3545–3555.
[37] P. Hao, Z. Zhao, Y. Leng, J. Tian, Y. Sang, R.I. Boughton, C. Wong, H. Liu, B. Yang, Graphene-based nitrogen self-doped hierarchical porous carbon aerogels derived from chitosan for high performance supercapacitors, Nano Energy 15 (2015) 9–23.
[38] C. Koczwara, S. Rumswinkel, C. Prehal, N. Jäckel, M.S. Elsaesser, H. Amenitsch, V. Presser, N. Hüsing, O. Paris, In situ measurement of electrosorption-induced deformation reveals the importance of micropores in hierarchical carbons, ACS Appl. Mater. Interfaces 9 (28) (2017) 23319–23324.
[39] L.P. Ramírez, K. Landfester, Magnetic polystyrene nanoparticles with a high magnetite content obtained by miniemulsion processes, Macromol. Chem. Phys. 204 (1) (2003) 22–31.